7-1-2017

A descriptive and broadly applicable model of therapeutic and stray absorbed dose from 6 to 25 MV photon beams:

Christopher W. Schneider
Louisiana State University

Wayne D. Newhauser
Louisiana State University

Lydia J. Wilson
Louisiana State University

Uwe Schneider
Universität Zürich

Robert Kaderka
GSI Helmholtz Centre for Heavy Ion Research GmbH

See next page for additional authors

Recommended Citation

Schneider, C., Newhauser, W., Wilson, L., Schneider, U., Kaderka, R., Miljanic, S., Kneževic, Ž., Stolarcyzk, L., Durante, M., & Harrison, R. (2017). A descriptive and broadly applicable model of therapeutic and stray absorbed dose from 6 to 25 MV photon beams:. *Medical Physics, 44* (7), 3805-3814. https://doi.org/10.1002/mp.12286

PATIENT QA, MACHINE QA, DEVICES AND DATA — ALL IN ONE PLACE

SunCHECK™

With a single interface and a single database, SunCHECK will cover:

- Dose**CHECK**™ - Independent secondary 3D dose calculations
- Per**FRACTION**™ **Fraction 0**™ - Phantom-less 2D and 3D pre-treatment QA
- Per**FRACTION**™ **Fraction n**™ - 3D transit/in-vivo monitoring
- SNC **Machine**™ - TG-142/VMAT imaging and mechanical QA
- SNC **Routine**™ - Daily, monthly and annual test management, with live device integration COMING SOON

This is precisely the kind of QA innovation you can always expect from Sun. Innovations that help improve outcomes and workflow efficiency, with ease.

sunnuclear.com

SUN NUCLEAR corporation

A descriptive and broadly applicable model of therapeutic and stray absorbed dose from 6 MV to 25 MV photon beams

Christopher W. Schneider, Wayne D. Newhauser,* and Lydia J. Wilson

Department of Physics and Astronomy,

Louisiana State University and Agricultural and

Mechanical College, Baton Rouge, LA 70803-4001

Uwe Schneider†

Faculty of Science, University of Zürich,

Winterthurerstrasse 260, 8057 Zürich, Switzerland

Robert Kaderka

GSI Helmholtzzentrum für Schwerionenforschung,

Department of Biophysics, Darmstadt 64291, Germany

Saveta Miljanić and Željka Knežević

Ruđer Bošković Institute, Radiation Chemistry and Dosimetry Laboratory,

Bijenička 54, HR-10000 Zagreb, Croatia

Liliana Stolarcyzk

Bronowice Cyclotron Centre, Institute of Nuclear Physics PAN,

Radzikowskiego 152, 31-342 Krakow, Poland

Marco Durante

Trento Institute for Fundamental Physics and

Applications—INFN, 38123 Povo, Trento, Italy

Roger M. Harrison

University of Newcastle, Faculty of Medical Sciences,

Newcastle upon Tyne NE2 4HH, UK

(Dated: April 17, 2017)

Abstract

Purpose: To develop a simple model of therapeutic and stray absorbed dose for a variety of treatment machines and techniques without relying on proprietary machine-specific parameters.

Methods: Dosimetry measurements conducted in this study and from the literature were used to develop an analytical model of absorbed dose from a variety of treatment machines and techniques in the 6 MV to 25 MV interval. A modified one-dimensional gamma-index analysis was performed to evaluate dosimetric accuracy of the model on an independent dataset consisting of measured dose profiles from seven treatment units spanning four manufacturers.

Results: The average difference between the calculated and measured absorbed dose values was 9.9% for those datasets on which the model was trained. Additionally, These results indicate that the model can provide accurate calculations of both therapeutic and stray radiation dose from a wide variety of radiotherapy units and techniques.

Conclusions: We have developed a simple analytical model of absorbed dose from external beam radiotherapy treatments in the 6 MV to 25 MV beam energy range. The model has been tested on measured data from multiple treatment machines and techniques and is broadly applicable to contemporary external beam radiation therapy.

Keywords: out-of-field dose, absorbed dose, analytical model, external beam radiotherapy

* newhauser@lsu.edu; Mary Bird Perkins Cancer Center, 4950 Essen Lane, Baton Rouge, LA 70809

† Institute for Radiotherapy, Hirslanden Medical Center, Rain 34, 5000 Aarau, Switzerland

I. INTRODUCTION

The goal of modern external beam radiotherapy is to deliver a highly targeted radiation dose to a diseased anatomic location or region while sparing the the rest of the body. However, in practice, the whole body is unavoidably exposed to unwanted stray radiation. Healthy tissue in the margin of the treatment field will receive absorbed doses on the order of the prescribed dose. Tissues outside the treatment field receive stray dose from scattered and leakage radiation that is one to four orders of magnitude smaller [1]. Historically, clinical practices focused almost exclusively on in-field exposures because of their prime importance to curing primary cancers. In recent years, 5-year survival rates have supassed 69% for all cancers [2] and 80% for childhood cancers [3], but a myriad of radiation epidemiology studies have revealed the high prevalence of radiation-induced late effects including cardiac toxicity and radiogenic second cancers[4, 5]. Most radiogenic second cancers occur outside the therapeutic radiation field [6–10]. For these reasons, there is increasing interest in knowing the small stray radiation exposures to the whole body.

Many researchers have reported algorithms to model absorbed dose from external beam photon radiation therapy [11–14]. In general, these algorithms accurately predict exposures inside and immediately outside the high-dose treatment field. However, none of these algorithms have fully addressed the stray dose far from the treatment field. Stovall *et al.* described three main sources of stray radiation from external beam radiation therapy delivered with electron linear accelerators [15]. Radiation scattered from the treatment head, known as head scatter, is primarily important within about 10 cm from the field edge. Patient scatter is an important source up to around 30 cm from the field edge. Finally, leakage radiation emanates from the treatment enclosure and predominates the stray radiation dose beyond about 30 cm. Monte Carlo simulations have been a useful research tool for modeling stray dose [16–18], but these methods have not found use in clinical settings due to their complexity and long computational times. The feasibility of analytical models to predict stray dose from radiation therapy has been supported by several works [7, 19–25], but few attempts have been made at developing models accurate for both in-field and out-of-field doses. Jagetic and Newhauser reported on one such model that accurately predicts absorbed dose from therapeutic, scatter, and leakage radiation [26]. This model was evaluated only at 6 MV photon-beam energy, only for Conformal Radiation Therapy (CRT), and only for one

type of electron linear accelerator (Elekta, SL25, Stockholm). The study left open important questions. Firstly, is this approach extensible to other treatment techniques, e.g., Intensity Modulated Radiation Therapy (IMRT)? Secondly, is it adaptable to treatment units from other manufacturers? Third, can it be done without proprietary data?

The objective of this study was to determine whether a physics-based analytical modeling approach is applicable to a variety of treatment techniques and treatment units. More specifically, we characterized the dosimetric accuracy that can be achieved without the use of proprietary and machine-specific parameters to configure the model. In order to accomplish this, we developed a new analytical model that can be configured with measured dose profiles that are similar to those used for configuring commercial treatment planning systems. The model was tested using measured data from a variety of treatment machines and techniques in the 6 to 25 MV interval of photon beam energy.

II. METHODS AND MATERIALS

A. Analytical Model

The analytical model consists of four terms: one to model the therapeutic radiation dose and three to model sources of stray dose, or

$$D_{\mathrm{T}} = D_{\mathrm{P}} + D_{\mathrm{HS}} + D_{\mathrm{PS}} + D_{\mathrm{L}} \quad , \tag{1}$$

where D_{T} is the total dose from all sources, D_{P} is the primary dose term that models the therapeutic dose, D_{HS} is the first stray dose term that models dose from head scattered radiation, D_{PS} is the second stray dose term that models dose from patient scattered radiation, and D_{L} is the third stray dose term that models leakage radiation.

Consequently, simplicity and ease of use were of prime importance to the model's design. In particular, we designed it for ease and simplicity of configuration, e.g., by using non-proprietary data that can be quickly measured in most clinics. The model proposed in this work shares the major underlying physics and mathematical form as that of Jagetic and Newhauser, but it was radically simplified here to streamline the configuration process and to eliminate the use of proprietary data. As will become readily apparent later, these two features were of prime importance in configuring the model for multiple treatment techniques

and machines. Table I compares the two models and detailed descriptions of the terms from this work follow below.

The primary absorbed dose, D_{P}, for square and rectangular fields is given by

$$D_{\mathrm{P}} = A_{\mathrm{P}} \times C(x,z) \times C(y,z) \times TF_{\mathrm{P,w}}(x,y,z,E) \tag{2}$$

where A_{P} governs the amplitude of the primary dose on the central axis, $C(x,z)$ and $C(y,z)$ govern the width and lateral penumbrae of the beam in the x and y directions, x and y are the lateral distances from central-axis in the plane of calculation for the in- and cross-plane directions, and $TF_{\mathrm{P,w}}(x,y,z,E)$ is the transmission factor of the primary portion of the beam of nominal energy E at a point (x,y,z) in a phantom.

The C functions in (2) model the shape of the primary dose via the simple but realistic approach of using cumulative normal distributions, as in

$$C(x,z) = \frac{1}{2\pi\sigma^2(z)} \times \left\{ \int_{-\infty}^{x} \exp\left[\frac{-(x' + \bar{x}(z))^2}{2(\sigma_{\mathrm{P}}^2(z))} \right] dx' \right\} \times \left\{ 1 - \int_{-\infty}^{x} \exp\left[\frac{-(x' - \bar{x}(z))^2}{2(\sigma_{\mathrm{P}}^2(z))} \right] dx' \right\} \quad . \tag{3}$$

where $\sigma_{\mathrm{P}}(z)$ is the width parameter for the cumulative normal functions used to define the penumbra, and $\bar{x}_{\mathrm{P}}(z)$ and $\bar{y}_{\mathrm{P}}(z)$ are the centroids of the cumulative normals projected to depth z. These parameters are described in detail below.

The parameters $\sigma_{\mathrm{P}}(z)$, $\bar{x}(z)$, and $\bar{y}(z)$ are scaled with depth according to

$$\sigma_{\mathrm{P}}(z) = \sigma_{\mathrm{P},0} \times F_{\mathrm{P}}(z) \quad , \tag{4}$$

$$\bar{x}(z) = \bar{x}_{\mathrm{P},0} \times F_{\mathrm{P}}(z) \quad , \tag{5}$$

$$\bar{y}(z) = \bar{y}_{\mathrm{P},0} \times F_{\mathrm{P}}(z) \quad , \tag{6}$$

where $\sigma_{\mathrm{P},0}$ is the width parameter in the isocentric plane, $\bar{x}_{\mathrm{P},0}$ and $\bar{y}_{\mathrm{P},0}$ are the lateral field edge locations in the isocentric plane. $F_{\mathrm{P}}(z)$ is the scaling factor defined as

$$F_{\mathrm{P}}(z) = \frac{\mathrm{SSD} + d_{\mathrm{iso}} + (z - d_{\mathrm{iso}}) \times \alpha_{\mathrm{P}}}{\mathrm{SSD} + d_{\mathrm{iso}}} \quad , \tag{7}$$

where SSD is the source-to-surface distance, d_{iso} is the depth at isocenter, and α_{P} is an empirical correction factor to the rate at which $\sigma_{\mathrm{P}}(z)$, $\bar{x}_{\mathrm{P}}(z)$, and $\bar{x}_{\mathrm{P}}(z)$ change with depth.

The transmission factor in water at the calculation point is given by

$$TF_{\mathrm{P,w}}(x,y,z,E) = \exp\left[-\mu_{\mathrm{P,eff}} \times d(x,y,z) \right] \quad , \tag{8}$$

TABLE I. Comparison of model terms for Jagetic and Newhauser [26] and this work.

	Jagetic and Newhauser [26]		This Work	
Term	Description	Eqn.	Description	Eqn.
Uncollimated Fluence, Φ	Modeled using electron radiation yield, 3 Gaussian source terms, and divergence.	(2.8)	Not modeled.	N/A
In-air Primary Collimated Fluence, Φ_{P}	Uncollimated fluence multiplied by cumulative normal.	(2.10)	Implicitly modeled.	(2)
Primary Dose in Water, $D_{\mathrm{P,w}}$	In-air primary fluence multiplied by transmission factor and mass-energy absorption coefficent.	(2.15)	Cumulative normal multiplied by transmission factor and primary scaling factor.	(2)
Leakage Fluence, Φ_{L}	Uncollimated fluence multiplied by complimentary cumulative normal.	(2.17)	Implicitly modeled.	(18)
Leakage Dose in Water, $D_{\mathrm{L,w}}$	Leakage fluence multiplied by transmission factors for collimators and water and mass-energy absorption coefficient.	(2.20)	Cumulative normal multiplied by Gaussian source term, water transmission factors, and energy dependent leakage scaling factor.	(18)
Head-Scatter Dose in Water, $D_{\mathrm{HS,w}}$	Gaussian multiplied by empirical, field-size dependent, scaling factor and water transmission factor.	(2.27)	Gaussian multiplied by energy-dependent scaling factor and water transmission factor.	(11)
Patient-Scatter Dose in Water, $D_{\mathrm{PS,w}}$	Dual Gaussians multiplied by empirical, field-size dependent scaling factors and water transmission factor.	(2.28)	Gaussian multiplied by energy-dependent scaling factor and water transmission factor.	(14)

where the path length through water to point (x, y, z) is

$$d(x, y, z) = \sqrt{(\text{SSD} + z)^2 + x^2 + y^2} \times \left(\frac{z}{\text{SSD} + z}\right) \quad . \tag{9}$$

The effective linear photon attenuation coefficient is

$$\mu_{\text{P,eff}}(E) = (m_{\mu,\text{P}} \times E + b_{\mu,\text{P}}) \times \mu|_{\text{w},\bar{E}} \quad , \tag{10}$$

where $\mu_{\text{P,eff}}(E)$ is the effective linear attenuation coefficient in water for the primary portion of a beam of nominal energy E, and $\mu|_{\text{w},\bar{E}}$ is the linear attenuation coefficient in water for photons of energy $\bar{E}$, where $\bar{E}$ is the average energy of the photon beam approximated as one third the value of the nominal energy following Jagetic and Newhauser [26]. The parameters $b_{\mu,\text{P}}$ and $m_{\mu,\text{P}}$ are the 0^{th} and 1^{st} order coefficients, respectively, of an empirical correction factor to the effective linear attenuation coefficient that is parameterized with energy. This factor is needed because $\mu|_{\text{w},\bar{E}}$ will not equal the true energy weighted mean of the linear attenuation coefficient, $\mu(E)$, across the full energy spectrum of the beam. The values of the parameters $b_{\mu,\text{P}}$ and $m_{\mu,\text{P}}$ are determined along with the other fitting parameters via the model training procedure described in Section II C. The values of $\mu|_{\text{w},\bar{E}}$ for the energies considered in this study were found from the National Institute of Standards and Technology (NIST) XCOM photon cross sections database [27].

The stray dose is the sum of three terms. The head scatter dose term is the narrowest laterally and is given by

$$\begin{aligned} D_{\text{HS}}(x, y, z, E) = \frac{A_{\text{HS}}(E)}{\sigma_{\text{HS}}(z)\sqrt{2\pi}} \exp\left[\frac{-(x^2 + y^2)}{2\sigma_{\text{HS}}^2(z)}\right] \\ \times TF_{\text{HS,w}}(x, y, z, E) \quad , \end{aligned} \tag{11}$$

where $A_{\text{HS}}(E)$ is the energy dependent scaling factor given by

$$A_{\text{HS}}(E) = \beta_{\text{HS}} \times E + \gamma_{\text{HS}} \quad , \tag{12}$$

β_{HS} and γ_{HS} are the 1^{st} and 0^{th} order coefficients, respectively, that parameterize the factor with photon beam energy. The depth dependent width parameter, $\sigma_{\text{HS}}(z)$, is given by

$$\sigma_{\text{HS}}(z) = \sigma_{\text{HS},0} \times F_{\text{HS}}(z) \quad , \tag{13}$$

where $\sigma_{\text{HS},0}$, is the head scatter width parameter in the isocentric plane, $F_{\text{HS}}(z)$ is defined similarly to (7) with empirical adjustment factor α_{HS} , and $TF_{\text{HS,w}}(x, y, z, E)$ is the transmission factor for head scattered radiation defined similarly to (8).

The patient scatter dose term is similarly given by

$$D_{\mathrm{PS}}(x,y,z,E) = \frac{A_{\mathrm{PS}}(E)}{\sigma_{\mathrm{PS}}(z)\sqrt{2\pi}} \exp\left[\frac{-(x^2+y^2)}{2\sigma_{\mathrm{PS}}^2(z)}\right] \times TF_{\mathrm{PS,w}}(x,y,E) \quad , \tag{14}$$

where $A_{\mathrm{PS}}(E)$ is the energy dependent scaling factor

$$A_{\mathrm{PS}}(E) = \beta_{\mathrm{PS}} \times E + \gamma_{\mathrm{PS}} \quad , \tag{15}$$

β_{PS} and γ_{PS} are the 1^{st} and 0^{th} order coefficients, respectively, that parameterize the scaling factor with photon beam energy, and $\sigma_{\mathrm{PS}}(z)$ is a depth dependent width parameter that scales with depth according to

$$\sigma_{\mathrm{PS}}(z) = \sigma_{\mathrm{PS},0} \times F_{\mathrm{HS}}(z) \quad , \tag{16}$$

where $\sigma_{\mathrm{PS},0}$ is the head scatter width parameter in the isocentric plane and $F_{\mathrm{PS}}(z)$ is defined similarly to (7) with empirical adjustment factor α_{PS}. The transmission factor for radiation from patient scatter in a water phantom is given by

$$TF_{\mathrm{PS,w}}(x,y,E) = \exp\left(-\mu_{\mathrm{PS,eff}}(E) \times \sqrt{x^2+y^2}\right) . \tag{17}$$

The functional form of the leakage dose term is illustrated in Figure 1 and is defined as

$$D_{\mathrm{L}}(x,y,z,E) = \frac{A_{\mathrm{L}}(E)}{\sigma_{\mathrm{L}}(z)\sqrt{2\pi}} \exp\left[\frac{-(x^2+y^2)}{2\sigma_{\mathrm{L}}^2(z)}\right] \times TF_{\mathrm{L,w}}(x,y,z,E) \times PC(r,z,E) \times [1 - C(x,z) \times C(y,z)] \quad , \tag{18}$$

where $A_{\mathrm{L}}(E)$ is an energy dependent scaling factor

$$A_{\mathrm{L}}(E) = (\beta_{\mathrm{L}} \times E + \gamma_{\mathrm{L}})\, F_{\phi} \quad , \tag{19}$$

and F_{ϕ} accounts for increased leakage present in treatments with large amount of photon fluence modulation. The depth-dependent width parameter from (18) is

$$\sigma_{\mathrm{L}}(z) = \sigma_{\mathrm{L},0} \times F_{\mathrm{L}}(z) \quad , \tag{20}$$

where $F_{\mathrm{L}}(z)$ is defined similarly to (7) with a corresponding empirical adjustment factor α_{L}. The factor $[1 - C(x,z) \times C(y,z)]$ suppresses the leakage term inside the treatment field, and

$PC(r,z,E)$ models attenuation in the primary collimator. This primary collimator function is given by

$$PC(r,z,E) = 1 - A_{\rm PC}(E) \times \int_{-\infty}^{r} \exp\left[\frac{-(r' + \bar{r}(z))^2}{2\sigma_{\rm PC}^2}\right] dr' \ , \tag{21}$$

where $r = \sqrt{x^2 + y^2}$, $A_{\rm PC}(E)$ is the energy dependent scaling factor

$$A_{\rm PC}(E) = \beta_{\rm PC} \times E + \gamma_{\rm PC} \quad , \tag{22}$$

$\sigma_{\rm PC}(z)$ is the width parameter of primary collimator penumbra given by

$$\sigma_{\rm PC}(z) = \sigma_{\rm PC,0} \times F_{\rm L}(z) \quad , \tag{23}$$

and $\bar{r}(z)$ is the lateral location of the primary collimator projected to depth z as in

$$\bar{r}(z) = \bar{r}_0 \times F_{\rm L}(z) \quad . \tag{24}$$

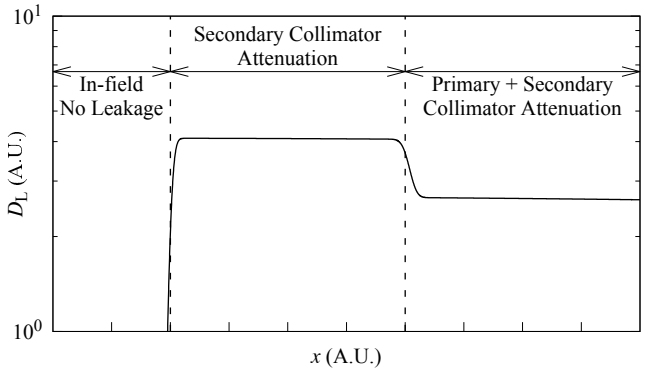

FIG. 1. Functional form of the leakage dose, $D_{\rm L}$, versus off-axis distance, x. In the in-field region, the leakage dose is defined to be zero. In the intermediate region, leakage is attenuated by the secondary collimator. Far out of field, there is additional attenuation from the primary collimator.

B. Measurements

There are three distinct sets of measured dosimetric data considered in this manuscript summarized in Table II. The first set was obtained in this study under the auspices of the

European Radiation Dosimetry (EURADOS) Working Group 9 (WG9), a multinational collaboration of institutions and researchers dedicated to research and development in the field of radiation dosimetry in medicine [1]. These experiments were specifically designed to yield dosimetric data that was needed to understand and model the physics of stray radiation exposure. The measurement methods and a limited number of preliminary results were previously reported by Bordy *et al* [28] The EURADOS data set consists of measurements made with multiple types thermoluminescent dosimeters (TLDs), radiophotoluminescent dosimeters (RPLs), and optically stimulated luminescent dosimeters (OSLDs) of doses delivered by a Saturne 43 linac (GE Medical Systems, USA). The calibration procedure for the various types of dosimeters is described by Knežević *et al* [29]. Doses were measured at various locations inside a 30 x 30 x 60 cm^3 water phantom. This data set includes dose profiles at 10, 15, 20, and 25 cm depths in water with a source-to-surface distance (SSD) of 90 cm, a field size of 10 x 10 cm^2, and beam energies of 6, 12, and 20 MV. The irradiations each delivered a reference dose of 2 Gy to the isocenter located at 10 cm depth. The measurements from this data set are being prepared for distribution in the form of electronic files containing complete tables of all numerical data and will be available for download from the EURADOS website (http://www.eurados.org).

TABLE II. Manufacturers, machines, techniques, nominal photon energies, and measurement phantoms considered in this study.

Data Set	MFR.	Model	Technique	Beam Energy (MV)	Phantom
EURADOS	GE	Saturne 43	CRT	6,12, 20	Water Box
KGU	Elekta	SL25	CRT	6, 18, 25	Water Box
(Halg *et al.*)	Varian	Clinac 21 iX	CRT, IMRT	6	Anthropomorphic
	Elekta	Synergy	IMRT	6	Anthropomorphic
	Siemens	Oncor Avant-Garde	IMRT	6	Anthropomorphic
		Mevatron Primus	Wedge		
	Accuray	CyberKnife	Stereotactic	6	Anthropomorphic
		TomoTherapy Hi-Art 2	IMRT		

The second data set used in this work comprises measurements performed at the Klinikum Goethe Universität (KGU) in Frankfurt, Germany. The KGU data set measurements were

made with a diamond detector model (60003 PTW, Freiburg) of doses delivered by an SL25 linac (Elekta, Stockholm) for various field sizes, depths, and beam energies. For this work, we consider 10 x 10 cm^2 fields at depths of 1.5 and 3.5 cm in water and 100 cm SSD for beam energies of 6, 18, and 25 MV. These measurements were previously published in Kaderka *et al* [30].

The third data set used in this work comprises doses measured in an anthropomorphic phantom (Alderson-Rando, RSD Radiology Support Devices, Long Beach, CA) for a variety of widely used treatment machines and treatment techniques. These measurements were previously published in Halg *et al* [31]. Prostate treatment plans were created for nine treatment techniques from four manufacturers, including Accuray (Sunnyvale, CA, USA), Elekta (Stockholm, Sweden), Varian Medical Systems (Palo Alto, CA, USA), and Siemens (Berlin, Germany). All beams in this data set had a nominal energy of 6 MV. The dose measurements were performed using TLDs placed inside the anthropomorphic phantom. The dose along the medial patient axis was determined using 34 TLDs spaced at 2.5 cm intervals from the target (in prostate) to the head.

C. Model Training

In this work, the analytical model was trained separately using the EURADOS and KGU data sets. Training was accomplished by simultaneously fitting the parameters listed in Table V to measured dose values at all locations and at all beam energies. We used a gradient search algorithm to vary the free parameters and minimize the sum of the local relative differences, ΔD_{Total}, between the predicted and measured values. The sum of total relative differences was defined according to

$$\Delta D_{\text{Total}} = \sum_{i=1}^{n} \Delta D_i = \sum_{i=1}^{n} \left[\frac{|D_i^{\text{model}} - D_i^{\text{measured}}|}{\left(D_i^{\text{model}} + D_i^{\text{measured}}\right)/2} \right] \quad , \tag{25}$$

where n is the number of data points. In order to characterize the goodness of fit, we calculated

$$\overline{\Delta D} = \Delta D_{\text{Total}}/n \quad , \tag{26}$$

where $\overline{\Delta D}$ is the average local relative difference, and

$$\Delta D_{\text{max}} = \max\left(\{\Delta D_1, ..., \Delta D_n\}\right) \quad , \tag{27}$$

where ΔD_{max} is the maximum of the local relative differences.

D. Model Validation

The model, as configured and trained on both the KGU and EURADOS data sets, was validated by comparison with independent data, namely, the measured dose profiles in an anthropomorphic phantom for several treatment machines and techniques. Variations in depth due to the irregular surface contour of the phantom were modeled implicitly since it has been demonstrated that these variations are modest [24]. We compared the model as trained on two independent training data sets in order to test the sensitivity of the agreement to the choice of training data.

The quality assurance technique known as gamma analysis, first described by Low *et al* [32], characterizes the agreement between measured and calculated dose distributions on a point by point basis by combining dose difference and distance to agreement criteria. In most radiotherapy clinics, the dose difference criterion is selected at 3% of the maximum dose, and the distance to agreement criterion at 3 mm. These values are commonly known as the Van Dyk criteria [33]. However, this choice is not suitable for application far outside of the treatment field since dose in this region is well under 3% of the maximum dose, rendering the test insensitive to important dose errors in the out-of-field region. To overcome this limitation, we extended the gamma index analysis method that is extended in order to provide sufficient sensitivity and dynamic range to characterize dosimetric agreement in both the in-field and out-of-field regions.

The gamma indices at all positions in therapeutic and out-of-field dose regions were calculated according to

$$\Gamma(x_{\mathrm{m}}, x_{\mathrm{c}}) = \begin{cases} \sqrt{\frac{r^2(x_{\mathrm{m}},x_{\mathrm{c}})}{\Delta d_{\mathrm{T}}^2} + \frac{\delta_{\mathrm{R}}^2(x_{\mathrm{m}},x_{\mathrm{c}})}{\Delta D_{\mathrm{R}}^2}}, & x_{\mathrm{m}} \text{ in/near field} \\ \sqrt{\frac{r^2(x_{\mathrm{m}},x_{\mathrm{c}})}{\Delta d_{\mathrm{OOF}}^2} + \frac{\delta_{\mathrm{A}}^2(x_{\mathrm{m}},x_{\mathrm{c}})}{\Delta D_{\mathrm{A}}^2}}, & x_{\mathrm{m}} \text{ out-of-field} \end{cases} \tag{28}$$

where x_{m} and x_{c} are the locations of measured and calculated dose values, respectively. $r(x_{\mathrm{m}}, x_{\mathrm{c}})$ is the difference in position between measured and calculated dose values, Δd_{T} and Δd_{OOF} are the distance to agreement criteria in the therapeutic and out-of-field regions, respectively, $\delta_{\mathrm{R}}(x_{\mathrm{m}}, x_{\mathrm{c}})$ represents the relative dose difference between measured and calculated dose values, ΔD_{R} is the relative dose difference criterion, $\delta_{\mathrm{A}}(x_{\mathrm{m}}, x_{\mathrm{c}})$ represents the absolute dose difference between measured and calculated dose values, and ΔD_{A} is the absolute dose difference criterion. The therapeutic dose region was delineated from the

out-of-field dose region at the 1% relative dose level based on previously published findings [26, 34–36]. This allows for a significantly more severe dosimetric test out-of-field than conventional methods. Gamma index analysis was performed separately comparing the analytical model calculations on each of the two training data sets to the anthropomorphic phantom data set for the Varian Clinac 21 iX CRT. Gamma index pass rates were selected at 100%, 95%, 90%, and 67%. The corresponding gamma index criteria were iteratively decreased until the analysis yielded the selected pass rate.

III. RESULTS

A. Model Training

Figure 2 shows the Elekta SL25 measured and analytical model calculated total absorbed dose values for the three nominal beam energies (6, 18, and 25 MV) from the KGU data set. This figure demonstrates excellent agreement between measurement and analytical model calculations across the range of nominal beam energies considered. Figure 3 shows the measured absorbed dose from the 6 MV beam at a depth 1.5 cm in water plotted with the analytical model calculated absorbed dose. The individual analytical model dose terms (*i.e.* D_{P}, D_{HS}, D_{PS}, D_{L}) are also plotted thus demonstrating how the combination of these terms yields excellent agreement in both the in- and out-of-field regions. Table III shows the average and local relative differences for the model compared with the KGU dataset including the 6 MV beam at a depth of 1.5 cm and the 18 and 25 MV beams each at a depth of 3.5 cm. The average local relative difference, defined in (26), was 9.9%. The maximum local relative difference, defined in (27), was 33%.

TABLE III. Average and maximum local relative differences for all nominal photon beam energies E for the model calculations compared with the Klinikum Goethe Universität (KGU) data set.

E	$\overline{\Delta D}(\%)$	$\Delta D_{\max}(\%)$
6 MV	7.1	23.9
18 MV	12.3	32.9
25 MV	8.1	33.0
All Energies	9.9	33.0

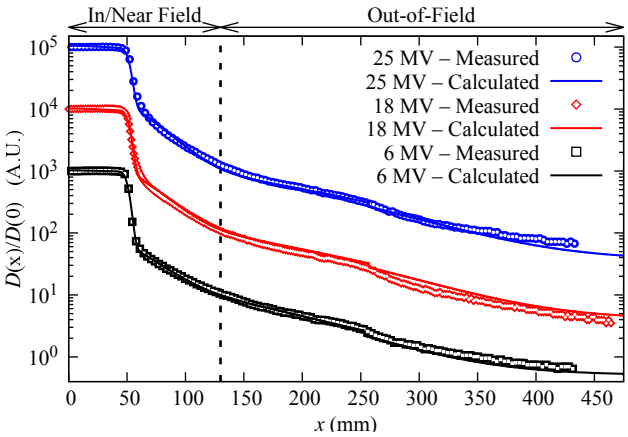

FIG. 2. Measured and calculated relative absorbed dose $D(x)/D(0)$ versus off-axis position x for all beam energies from the Klinikum Goethe Universität (KGU) data set. The abscissa corresponds to the lateral distance from the central axis of the beam. The ordinate represents the relative absorbed dose as a function of x. All profiles are at $d_{\max}$ (1.5 cm for 6 MV and 3.5 cm for 18 and 25 MV) and were normalized to the value of dose at $x = 0$. For visual clarity, the profiles are offset by factors of 10.

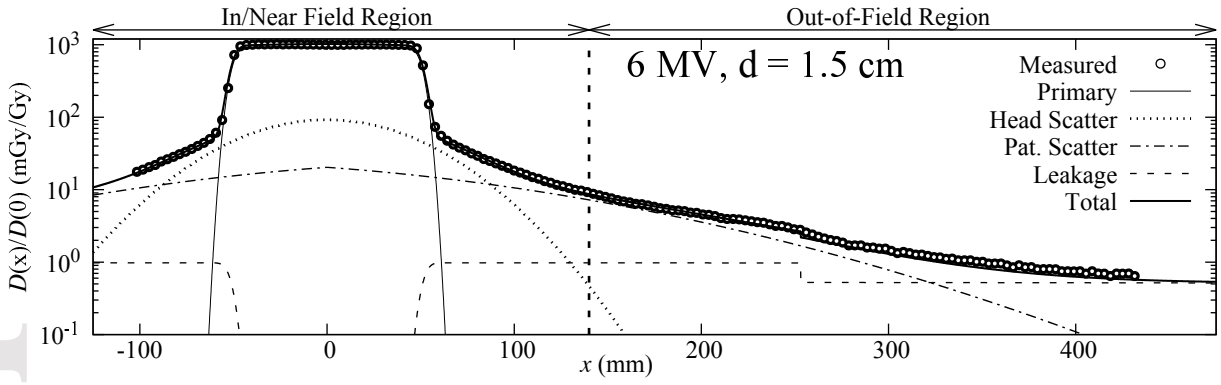

FIG. 3. Measured and calculated relative absorbed dose $D(x)/D(0)$ versus off-axis position x from the 6 MV beam at 1.5 cm depth in water from the Klinikum Goethe Universität (KGU) data set.

Figure 4 shows plots of Saturne 43 measured and analytical model calculated absorbed dose for the 6, 12, and 20 MV nominal beam energies at depths in water of 10 and 25 cm from the model as trained with the EURADOS data set. Very good agreement is seen between the model and the training data, showcasing the ability of the model to accurately calculate absorbed dose across a range of energies and depths. Figure 5 show the measured absorbed

dose from the 6 MV beam at a depth 10 cm in water plotted with the analytical model calculated absorbed dose and all individual dose components. Table IV lists the average and maximum local relative differences for all energies and depths included in this data set. The average difference for all locations and energies considered was 9.9% and the maximum difference was 41%.

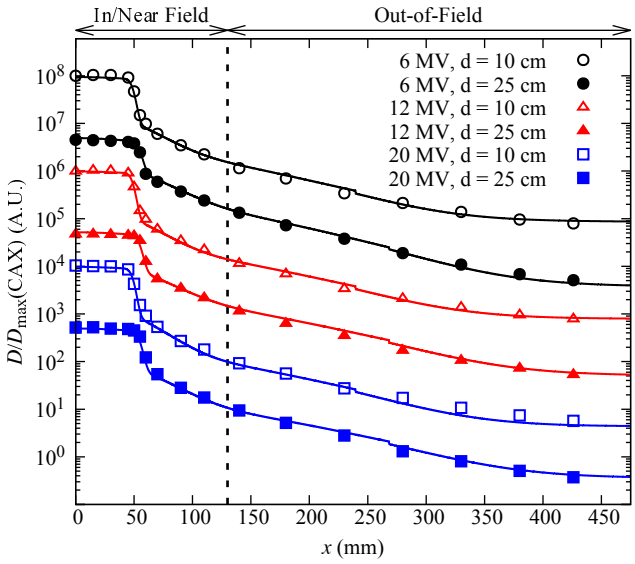

FIG. 4. Measured and calculated relative absorbed dose $D(x)/D_{\text{iso}}$ versus off-axis position x for 6, 12, and 20 MV beams at 10 cm and 25 cm depths in water from the European Radiation Dosimetry Group (EURADOS) data set. The abscissa corresponds to distance from the central axis of the beam. The ordinate corresponds to the relative absorbed dose as a function of x. The profiles were normalized to the value of dose at isocenter for the given beam energy. For visual clarity, the profiles were offset from one another by factors of 10.

The model parameter values resulting from fitting the model to the KGU and EURADOS data sets of measurements in water are listed in Table V. The relative differences between the parameters as fit on these data sets are also listed. The primary dose parameters resulting from fitting the model to each of the two data sets are similar with no parameter differing by more than 33.5%. However, there are considerable differences between the parameters for the out-of-field dose components, thus highlighting the ability of the model to adapt to out-of-field dose profiles of different machines.

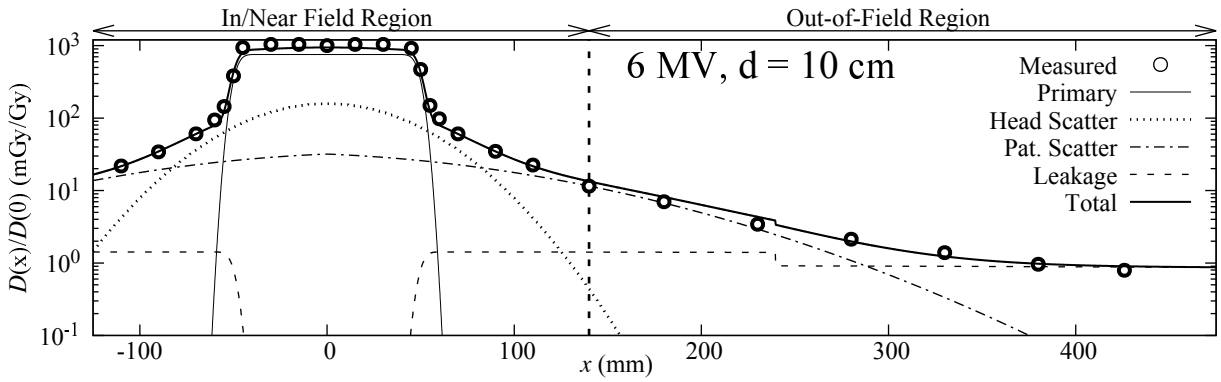

FIG. 5. Measured and calculated relative absorbed dose $D(x)/D(0)$ versus off-axis position x for the 6 MV beam at 10 cm depth in water from European Radiation Dosimetry Group (EURADOS) data set.

TABLE IV. Average and maximum local relative differences for all nominal photon beam energies and depths for the model calculations compared with the European Radiation Dosimetry Group (EURADOS) data set.

	6 MV		12 MV		20 MV		All Energies	
Depth (cm)	$\overline{\Delta D}$(%)	$\Delta D_{\max}$(%)	$\overline{\Delta D}$(%)	$\Delta D_{\max}$(%)	$\overline{\Delta D}$(%)	$\Delta D_{\max}$(%)	$\overline{\Delta D}$(%)	$\Delta D_{\max}$(%)
10	10.2	26.9	10.3	25.2	11.8	30.7	10.8	30.7
15	11.8	31.2	9.5	27.9	10.6	34.6	10.6	34.6
20	9.8	41	7.4	20.3	9.1	31.7	8.7	41
25	8.6	30.3	8.8	26.5	10.8	27.4	9.4	30.3
All depths	10.1	41	9	27.9	10.6	34.6	9.9	41

B. Validation with anthropomorphic phantom measurements

Doses measured in an anthropomorphic phantom for all nine treatment machines considered are shown in Figure 6. Also shown on this plot are the calculated doses from the analytical model as trained on both the KGU and EURADOS data sets from the previous section. The gamma index criteria required to achieve the selected passing rates are listed in Table VI.

The large differences in leakage radiation seen in the measured profiles in Figure 6 are due to differences in the fluence modulation used for the different techniques, as well as variations

TABLE V. Model parameters for model as trained on Klinikum Goethe Universität (KGU) and European Radiation Dosimetry Group (EURADOS) data sets and the relative differences between the results for each.

Term	Description	Symbol	KGU	EURADOS	Rel. Diff.
Primary	Dose coefficient	A_{P} (mGy/Gy)	982	1326	29.9%
	Field edge	$\bar{x}_{\mathrm{P},0}$ (cm)	5.0	4.9	1.4%
	Penumbra	$\sigma_{\mathrm{P},0}$ (cm)	0.33	0.33	1.6%
	Projection correction factor	α_{P} (—)	1.1	0.78	33.5%
	Attenuation 0^{th} order coefficient	$b_{\mu,\mathrm{P}}$ (—)	0.7	0.8	13.7%
	Attneuation 1^{st} order coefficient	$m_{\mu,\mathrm{P}}$ (MeV^{-1})	5.2×10^{-2}	5.7×10^{-2}	8.5%
Head Scatter	Dose 0^{th} order coefficient	β_{HS} (mGy/Gy)	5592	14619	89.3%
	Dose 1^{st} order coefficient	γ_{HS} (mGy/Gy/MeV)	722	263	93.3%
	Width parameter	$\alpha_{\mathrm{HS},0}$ (cm)	4.2	4.1	4.0%
	Projection correction factor	α_{HS} (—)	0.88	0.79	10.8%
	Attenuation 0^{th} order coefficient	$b_{\mu,\mathrm{HS}}$ (—)	-0.2	-0.3	34.3%
	Attneuation 1^{st} order coefficient	$m_{\mu,\mathrm{HS}}$ (MeV^{-1})	3.5×10^{-2}	5.0×10^{-2}	35.6%
Patient Scatter	Dose 0^{th} order coefficient	β_{PS} (mGy/Gy)	8586	11666	30.4%
	Dose 1^{st} order coefficient	γ_{PS} (mGy/Gy/MeV)	-145	-342	80.9%
	Width parameter	$\alpha_{\mathrm{PS},0}$ (cm)	15.0	12.0	21.9%
	Projection correction factor	α_{PS} (—)	0.60	0.58	3.6%
	Attenuation 0^{th} order coefficient	$b_{\mu,\mathrm{PS}}$ (—)	0.98	0.58	51.0%
	Attneuation 1^{st} order coefficient	$m_{\mu,\mathrm{PS}}$ (MeV^{-1})	-1.8×10^{-2}	-1.5×10^{-2}	13.7%
Leakage	Dose 0^{th} order coefficient	β_{L} (mGy/Gy)	10201	16967	49.8%
	Dose 1^{st} order coefficient	γ_{L} (mGy/Gy/MeV)	-100	-613	143.9%
	Width parameter	$\alpha_{\mathrm{L},0}$ (cm)	340	239	34.8%
	Projection correction factor	α_{L} (—)	0.80	0.80	0.7%
	Attenuation 0^{th} order coefficient	$b_{\mu,\mathrm{L}}$ (—)	2.02	1.20	51.1%
	Attneuation 1^{st} order coefficient	$m_{\mu,\mathrm{L}}$ (MeV^{-1})	-4.7×10^{-2}	-5.0×10^{-2}	6.6%
	PC 0^{th} order coefficient	β_{PC} (—)	0.44	0.33	29.3%
	PC 1^{st} order coefficient	γ_{PC} (MeV^{-1})	4.0×10^{-3}	3.5×10^{-3}	11.4%
	PC location	$\bar{x}_{\mathrm{PC}}$ (cm)	25.0	24.0	4.3%
	PC penumbra	σ_{PC} (cm)	5.0×10^{-3}	5.0×10^{-3}	0.0%

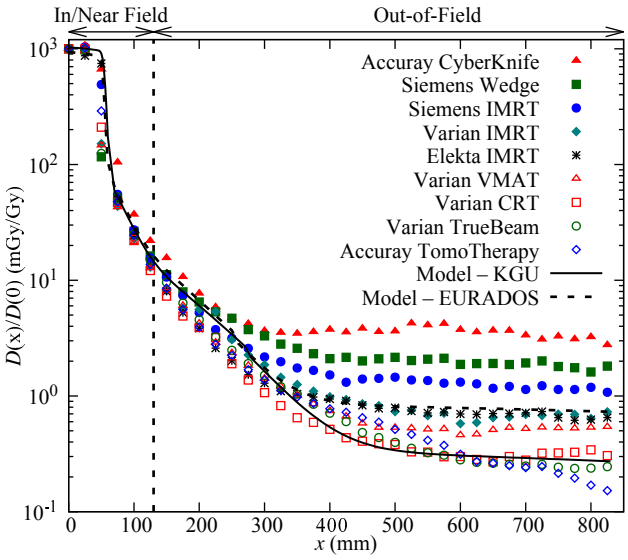

FIG. 6. Relative absorbed dose $D(x)/D(0)$ versus off-axis position x in anthropomorphic phantom from irradiations by various treatment techniques and machines. Points represent measured doses. Lines represent analytical model calculations from the model as trained on the Klinikum Goethe Universität (KGU) and European Radiation Dosimetry Group (EURADOS) data sets, respectively.

in collimators and head shielding in various machines. For example, the increased leakage from the CyberKnife unit was likely due to reduced head shielding in order to facilitate the mounting of the linac on a robotic arm. On the other hand, the increased leakage from the wedged field technique was due to the greater beam-on time required to produce wedged fields. Dose profiles from special techniques such as these should not be expected to closely match the dose profiles of more typical treatment techniques, *e.g.*, IMRT. By fitting the model parameters for each curve individually, it is possible to faithfully reproduce each of the measured dose profiles in a descriptive capacity (not shown), but additional development is necessary to extend the model to include explicit modeling of fluence modulation for predictive purposes.

IV. DISCUSSION

This work strongly suggests that there is potential for improving the completeness and accuracy of dose distribution calculations in routine clinical applications. The model is not

TABLE VI. Gamma index criteria for selected pass rates when comparing the model as trained on the Klinikum Goethe Universität (KGU) and European Radiation Dosimetry Group (EURADOS) data sets to the anthropomorphic phantom data set for the Varian Clinac 21 iX. The criteria considered include relative dose difference, ΔD_{R}; absolute dose difference, ΔD_{A}; and distance to agreement in the therapeutic and out-of-field regions, Δd_{t} and Δd_{OOF}, respectively.

		Therapeutic		Out-of-Field	
Training Data Set	Pass Rate	ΔD_{R} (%)	Δd_{t} (mm)	ΔD_{A} $\left(\frac{mGy}{Gy}\right)$	Δd_{OOF} (mm)
KGU	100	8	18	3.5	0.5
	95	6	14	3.1	0.5
	90	4	10	2.2	0.5
	67	3	7	0.3	0.5
EURADOS	100	15	20	4.5	0.5
	95	11	16	3.9	0.5
	90	8	12	2.5	0.5
	67	6	8	0.6	0.5

intended to replace current methods of treatment planning, but could be used in conjunction with current methods to provide a level of accuracy for the dose far outside the treatment field that is not available from currently available commercial treatment planning systems. With further study, this model could be implemented for use in hand calculations of fetal dose in the case of a pregnant radiation therapy patient or the dose to implants such pacemakers that may be damaged by radiation. Additionally, the ability to calculate therapeutic and stray radiation with a single model should be useful for studies in radiation epidemiology or as an educational tool for demonstrating the shape and relative magnitudes of the dose distributions from various treatment machines and techniques. Importantly, this may all be possible with a single analytical model that users may implement with measured data that is likely to already exist for their clinic.

The results of this study are coherent with previous works related to analytical models of total dose from external beam radiation therapy. In particular, the results achieved in

this work agree well with those of a more complex model previously reported by Jagetic and Newhauser [26]. The model offers simplicity, easy portability to various treatment machines and techniques, and increased speed compared with the more detailed model of Jagetic and Newhauser.

Major strengths of this study include the large number of treatment machines and techniques considered. Whereas previous works have been limited to single treatment techniques, this work considers nine techniques delivered with seven treatment machines from four manufacturers. This is made possible by the simplicity of the reported model. Additionally, in demonstrating the accuracies that are achievable with such a simple model, this work informs about the tradeoff between accuracy and complexity for analytical dose models.

Limitations of this work include the limited amount of measured data taken for each treatment technique. Additionally, only the descriptive capabilities of the model have been examined in this work, and the model's ability to predict doses for treatments with different setup conditions has not been tested. This is not a serious limitation because a lookup table approach could be used to apply this model to many different setup conditions with only a few measurements required. Another limitation of the model, in its current form, is the lack of photoneutrons at beam energies greater than 10 MV. However, this is not a serious limitation because most external beam photon treatments are delivered with 6 MV beams. This is especially true of IMRT. Additionally, for beam energies up to 18 MV, the component of equivalent dose due to photoneutrons is a small fraction of that due to leakage photons [30]. Also, the model can be extended to include photoneutrons in future studies. Other future work should include testing the model for dosimetric accuracy under different treatment conditions, such as field size. Additionally, implementing the model into a treatment planning system would allow for further testing of the practicality of using analytical models of stray dose in clinical settings. Our research group has recently performed similar work by implementing an analytical model of neutron dose from passively-scattered proton therapy into a research treatment planning system [37].

V. CONCLUSION

In this work we developed a new, broadly-applicable analytical model of the total dose from external beam radiation therapy. The model provides very good accuracy, on average

better than 10%, for both therapeutic and stray dose for a wide variety of treatment machines and techniques when compared with measured data. Importantly, the model developed here may be configured using non-proprietary configuration parameters and dosimetric data that is readily measurable in most clinics.

ACKNOWLEDGMENTS

We thank J.M. Bordy, I. Bessieres, A. Ostrowsky, B. Poumarede, S. Sorel, and D. Vermesse of CEA, Saclay for their contributions to the WG9 experiments. In particular, J.M. Bordy and I. Bessieres contributed substantially to this work and were invited to co-author this manuscript. Unfortunately, repeated efforts to contact them regarding this manuscript were unsuccessful. Hence, our acknowledgement of their contributions does not comprise their implicit endorsement of this manuscript.

DISCLOSURE OF CONFLICTS OF INTEREST

The authors have no relevant conflicts of interest to disclose.

[1] R. Harrison, "Introduction to dosimetry and risk estimation of second cancer following radiotherapy," *Radiat Meas*, vol. 57, pp. 1–8, 2013.

[2] R. L. Siegel, K. D. Miller, and A. Jemal, "Cancer statistics, 2016," *CA Cancer J Clin*, vol. 66, no. 1, pp. 7–30, 2016.

[3] N. Howlader, A. M. Noone, M. Krapcho, J. Garshell, D. Miller, and S. F. Altekruse, "Seer cancer statistics review, 1975-2011," report, National Cancer Institute, 2014.

[4] National Research Council, *Health Risks from Exposure to Low Levels of Ionizing Radiation: BEIR VII – Phase 2*. Washington, DC: The National Academies Press, 2006.

[5] NCRP, "Second primary cancers and cardiovascular disease after radiation therapy: NCRP Report No. 151." National Council on Radiation Protection and Measurements, Bethesda, Maryland, 2011.

[6] G. T. Armstrong, M. Stovall, and L. L. Robison, "Long-term effects of radiation exposure among adult survivors of childhood cancer: results from the childhood cancer survivor study," *Radiat Res*, vol. 174, no. 6, pp. 840–50, 2010.

[7] I. Diallo, A. Lamon, A. Shamsaldin, E. Grimaud, F. de Vathaire, and J. Chavaudra, "Estimation of the radiation dose delivered to any point outside the target volume per patient treated with external beam radiotherapy," *Radiother Oncol*, vol. 38, no. 3, pp. 269–71, 1996.

[8] W. D. Newhauser, A. Berrington de Gonzalez, R. Schulte, and C. Lee, "A review of radiotherapy-induced late effects research after advanced technology treatments," *Front Oncol*, vol. 6, p. 13, 2016.

[9] W. D. Newhauser and M. Durante, "Assessing the risk of second malignancies after modern radiotherapy," *Nat Rev Cancer*, vol. 11, no. 6, pp. 438–48, 2011.

[10] W. Dorr and T. Herrmann, "Cancer induction by radiotherapy: dose dependence and spatial relationship to irradiated volume," *J Radiol Prot*, vol. 22, no. 3A, pp. A117–21, 2002.

[11] A. Ahnesjo, "Collapsed cone convolution of radiant energy for photon dose calculation in heterogeneous media," *Med Phys*, vol. 16, no. 4, pp. 577–92, 1989.

[12] T. Han, J. K. Mikell, M. Salehpour, and F. Mourtada, "Dosimetric comparison of acuros xb deterministic radiation transport method with monte carlo and model-based convolution methods in heterogeneous media," *Med Phys*, vol. 38, no. 5, pp. 2651–64, 2011.

[13] T. R. Mackie, J. W. Scrimger, and J. J. Battista, "A convolution method of calculating dose for 15-mv x rays," *Med Phys*, vol. 12, no. 2, pp. 188–96, 1985.

[14] R. Mohan, C. Chui, and L. Lidofsky, "Differential pencil beam dose computation model for photons," *Med Phys*, vol. 13, no. 1, pp. 64–73, 1986.

[15] M. Stovall, C. R. Blackwell, J. Cundiff, D. H. Novack, J. R. Palta, L. K. Wagner, E. W. Webster, and R. J. Shalek, "Fetal dose from radiotherapy with photon beams: report of aapm radiation therapy committee task group no. 36," *Med Phys*, vol. 22, no. 1, pp. 63–82, 1995.

[16] A. Joosten, F. Bochud, and R. Moeckli, "A critical evaluation of secondary cancer risk models applied to monte carlo dose distributions of 2-dimensional, 3-dimensional conformal and hybrid intensity-modulated radiation therapy for breast cancer," *Phys Med Biol*, vol. 59, no. 16, pp. 4697–722, 2014.

[17] S. F. Kry, U. Titt, D. Followill, F. Ponisch, O. N. Vassiliev, R. A. White, M. Stovall, and M. Salehpour, "A monte carlo model for out-of-field dose calculation from high-energy photon

therapy," *Med Phys*, vol. 34, no. 9, pp. 3489–99, 2007.

[18] S. F. Kry, U. Titt, F. Ponisch, D. Followill, O. N. Vassiliev, R. A. White, R. Mohan, and M. Salehpour, "A monte carlo model for calculating out-of-field dose from a varian 6 mv beam," *Med Phys*, vol. 33, no. 11, pp. 4405–13, 2006.

[19] M. A. Benadjaoud, J. Bezin, A. Veres, D. Lefkopoulos, J. Chavaudra, A. Bridier, F. de Vathaire, and I. Diallo, "A multi-plane source model for out-of-field head scatter dose calculations in external beam photon therapy," *Phys Med Biol*, vol. 57, no. 22, pp. 7725–39, 2012.

[20] N. Chofor, D. Harder, K. C. Willborn, and B. Poppe, "Internal scatter, the unavoidable major component of the peripheral dose in photon-beam radiotherapy," *Phys Med Biol*, vol. 57, no. 6, pp. 1733–43, 2012.

[21] S. F. Kry, M. Salehpour, D. S. Followill, M. Stovall, D. A. Kuban, R. A. White, and I. Rosen, "Out-of-field photon and neutron dose equivalents from step-and-shoot intensity-modulated radiation therapy," *Int J Radiat Oncol Biol Phys*, vol. 62, no. 4, pp. 1204–16, 2005.

[22] M. Stovall, S. S. Donaldson, R. E. Weathers, L. L. Robison, A. C. Mertens, J. F. Winther, J. H. Olsen, and J. Boice, J. D., "Genetic effects of radiotherapy for childhood cancer: gonadal dose reconstruction," *Int J Radiat Oncol Biol Phys*, vol. 60, no. 2, pp. 542–52, 2004.

[23] M. Stovall, R. Weathers, C. Kasper, S. A. Smith, L. Travis, E. Ron, and R. Kleinerman, "Dose reconstruction for therapeutic and diagnostic radiation exposures: use in epidemiological studies," *Radiat Res*, vol. 166, no. 1 Pt 2, pp. 141–57, 2006.

[24] P. J. Taddei, W. Jalbout, R. M. Howell, N. Khater, F. Geara, K. Homann, and W. D. Newhauser, "Analytical model for out-of-field dose in photon craniospinal irradiation," *Phys Med Biol*, vol. 58, no. 21, pp. 7463–79, 2013.

[25] P. H. van der Giessen, "Peridose, a software program to calculate the dose outside the primary beam in radiation therapy," *Radiother Oncol*, vol. 58, no. 2, pp. 209–13, 2001.

[26] L. J. Jagetic and W. D. Newhauser, "A simple and fast physics-based analytical method to calculate therapeutic and stray doses from external beam, megavoltage x-ray therapy," *Phys Med Biol*, vol. 60, no. 12, pp. 4753–75, 2015.

[27] M. J. Berger, J. H. Hubbell, S. M. Seltzer, J. Chang, J. S. Coursey, R. Sukumar, Z. D. S, and K. Olsen, "XCOM: Photon Cross Section Database (version 1.5)." [Online] Available: http://physics.nist.gov/xcom. National Institute of Standards and Technology, Gaithersburg, MD., 2010.

[28] J. Bordy, I. Bessiere, E. d'Agostino, C. Domingo, F. d'Errico, A. di Fulvio, Ž. Knežević, S. Miljanić, P. Olko, A. Ostrosky, B. Poumarede, S. Sorel, L. Stolarczyk, V. D., and R. Harrison, "Radiotherapy out-of-field dosimetry: Experimental and computational results for photons in a water tank," *Radiat Meas*, vol. 57, pp. 29–34, 2013.

[29] Ž. Knežević, L. Stolarczyk, I. Bessieres, J. M. Bordy, S. Miljanić, and P. Olko, "Photon dosimetry methods outside the target volume in radiation therapy: Optically stimulated luminescence (osl), thermoluminescence (tl) and radiophotoluminescence (rpl) dosimetry," *Radiation Measurements*, vol. 57, pp. 9–18, 2013.

[30] R. Kaderka, D. Schardt, M. Durante, T. Berger, U. Ramm, J. Licher, and C. La Tessa, "Out-of-field dose measurements in a water phantom using different radiotherapy modalities," *Phys Med Biol*, vol. 57, no. 16, pp. 5059–74, 2012.

[31] R. A. Halg, J. Besserer, and U. Schneider, "Systematic measurements of whole-body dose distributions for various treatment machines and delivery techniques in radiation therapy," *Med Phys*, vol. 39, no. 12, pp. 7662–76, 2012.

[32] D. A. Low, W. B. Harms, S. Mutic, and J. A. Purdy, "A technique for the quantitative evaluation of dose distributions," *Med Phys*, vol. 25, no. 5, pp. 656–61, 1998.

[33] J. Van Dyk, R. B. Barnett, J. E. Cygler, and P. C. Shragge, "Commissioning and quality assurance of treatment planning computers," *Int J Radiat Oncol Biol Phys*, vol. 26, no. 2, pp. 261–73, 1993.

[34] R. M. Howell, S. B. Scarboro, S. F. Kry, and D. Z. Yaldo, "Accuracy of out-of-field dose calculations by a commercial treatment planning system," *Phys Med Biol*, vol. 55, no. 23, pp. 6999–7008, 2010.

[35] A. Joosten, O. Matzinger, W. Jeanneret-Sozzi, F. Bochud, and R. Moeckli, "Evaluation of organ-specific peripheral doses after 2-dimensional, 3-dimensional and hybrid intensity modulated radiation therapy for breast cancer based on monte carlo and convolution/superposition algorithms: implications for secondary cancer risk assessment," *Radiother Oncol*, vol. 106, no. 1, pp. 33–41, 2013.

[36] U. Schneider, R. A. Halg, M. Hartmann, A. Mack, F. Storelli, A. Joosten, R. Mockli, and J. Besserer, "Accuracy of out-of-field dose calculation of tomotherapy and cyberknife treatment planning systems: a dosimetric study," *Z Med Phys*, vol. 24, no. 3, pp. 211–5, 2014.

[37] J. Eley, W. Newhauser, K. Homann, R. Howell, C. Schneider, M. Durante, and C. Bert, "Implementation of an analytical model for leakage neutron equivalent dose in a proton radiotherapy planning system," *Cancers (Basel)*, vol. 7, no. 1, pp. 427–38, 2015.